SIAM J. SCI. COMPUT.
Vol. 42, No. 4, pp. B1041–B1066

AN FE-FD METHOD FOR ANISOTROPIC ELLIPTIC INTERFACE PROBLEMS*

BAIYING DONG†, XIUFANG FENG‡, AND ZHILIN LI§

Abstract. Anisotropic elliptic interface problems are important but hard to solve either analytically or numerically. There is limited literature on numerical methods based on structured meshes. Finite element methods are often used, but the usual average error estimates cannot guarantee accuracy of the solution near or at the interface. For finite difference methods, it is challenging to discretize mixed derivatives and carry out the convergence analysis. In this paper, a new finite element-finite difference (FE-FD) method that combines a finite element discretization (away from the interface) whose coefficient matrix is a symmetric semipositive definite, with a finite difference discretization (near or on the interface) whose coefficient matrix part has properties of an M-matrix, is developed. An interpolation scheme based on the immersed interface method is also applied to compute the normal derivative of solution (or gradient) accurately from each side of the interface. Error analysis and numerical experiments are also presented.

Key words. anisotropic elliptic interface problem, finite element and finite difference method, maximum principle preserving scheme, normal derivative computation, scaling technique, error analysis

AMS subject classifications. 65M06, 76M20, 65N06

DOI. 10.1137/19M1291030

1. Introduction.

A number of physical phenomena such as crystal growths, Hele–Shaw flows, etc. can be modeled by an anisotropic elliptic interface problem described below,

$$
\begin{aligned}
&-\nabla\cdot(\mathbf{A}(\mathbf{x})\nabla u(\mathbf{x}))+\sigma(\mathbf{x})u(\mathbf{x})=f(\mathbf{x}), \qquad \mathbf{x}\in\Omega\setminus\Gamma, \quad \Omega=\Omega^+\cup\Omega^-,\\
&\mathbf{A}(\mathbf{x})=\begin{pmatrix} A_{11}(\mathbf{x}) & A_{12}(\mathbf{x})\\ A_{12}(\mathbf{x}) & A_{22}(\mathbf{x})\end{pmatrix}\in C(\Omega\setminus\Gamma), \qquad u(\mathbf{x})\,\big|_{\partial\Omega}=u_0(x,y),
\end{aligned}
\tag{1}
$$

where $\mathbf{A}$ is a symmetric positive definite matrix whose eigenvalues satisfy, $\lambda_i(\mathbf{x})\geq\lambda_0>0$, $i=1,2$, for all $\mathbf{x}\in\Omega$; $\sigma(\mathbf{x})\geq 0$; $f(\mathbf{x})\in C(\Omega\setminus\Gamma)$ is a source term, and $\Gamma=\mathbf{X}(s)=(X(s),Y(s))\in C^2$ is an interface within the solution domain; see Figure 1 for an illustration. In the diagram, $\mathbf{A}^+(\mathbf{x})$ and $\mathbf{A}^-(\mathbf{x})$ are restrictions of $\mathbf{A}(\mathbf{x})$ on Ω^+ and Ω^-, respectively, that is,

$$
\mathbf{A}(\mathbf{x})=\begin{cases}\mathbf{A}^+(\mathbf{x}) & \text{if } \mathbf{x}\in\Omega^+,\\ \mathbf{A}^-(\mathbf{x}) & \text{if } \mathbf{x}\in\Omega^-.\end{cases}
$$

*Submitted to the journal's Computational Methods in Science and Engineering section October 3, 2019; accepted for publication (in revised form) April 20, 2020; published electronically August 11, 2020.

https://doi.org/10.1137/19M1291030

Funding: The first author's work was partially supported by the Foundation of NingXia Normal University grant NXSFZDA2002. The second author's work was partially supported by the CNSF grant 11961054. The third author's work was supported by a Simon's Foundation grant 633724.

†School of Mathematics and Statistics, NingXia University and School of Mathematics and Computer Science, NingXia Normal University, NingXia 750021, China (dongbaiying@126.com).

‡Co-corresponding author. School of Mathematics and Statistics, NingXia University, NingXia 750021, China (xf_feng@nxu.edu.cn).

§Corresponding author. CRSC and Department of Mathematics, North Carolina State University, Raleigh, NC 27695-8205 (zhilin@math.ncsu.edu).

Two jump conditions, also called internal boundary conditions—the jump in the solution and the flux below—are needed to close the system,

$$[u](\mathbf{X}) = w(s) \in C^2(\Gamma), \qquad [\mathbf{A}\nabla u \cdot \mathbf{n}](\mathbf{X}) = v(s) \in C^1(\Gamma), \qquad \mathbf{X} \in \Gamma, \tag{2}$$

where $\mathbf{X} = (X, Y)$ is a point on the interface Γ and $\mathbf{n}$ is the unit normal direction pointing to the outer boundary.

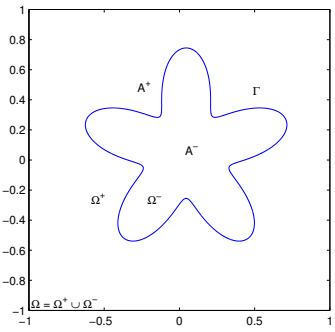

FIG. 1. *A diagram of a domain with an interface* Γ. *The domain is divided into* Ω^+ *and* Ω^- *separated by* Γ *across which physical quantities such as* $\mathbf{A}(\mathbf{x})$, $\sigma(\mathbf{x})$, *and* $f(\mathbf{x})$ *can be discontinuous.*

There are many discussions in the literature about anisotropic interface problems including physics and modeling [4, 20, 22], analysis [18, 26, 28], and numerical methods [1, 9, 16, 17].

The well-posedness of the problem has been well established based on the Lax–Milgram lemma. Most numerical methods are based on the Galerkin finite element formulation that guarantees the solvability of the discrete system when the regularity conditions are satisfied. When $\mathbf{A}$ is discontinuous across an interface Γ and the solution is continuous ($w = 0$), finite element methods (FEMs) using body fitted (unstructured) meshes work well. Nevertheless, sometimes methods based on structured meshes such as uniform or adaptive Cartesian ones are preferred. Advantages of these types of methods include (i) there is almost no cost in the mesh generation; (ii) there are many efficient packages/solvers and numerical methods which are designed for structure or Cartesian meshes. It is relatively easier to incorporate new methods using existing packages/solvers based on the same mesh. In this paper, we will use Cartesian meshes to solve the anisotropic interface problem.

We note that there are few finite difference methods in the literature for solving anisotropic partial differential equations (PDEs) due to the presence of the mixed derivative term $\frac{\partial^2 u}{\partial x \partial y} = u_{xy}$, which also complicates the stability and convergence analysis. The resulting linear system of equations using the central finite difference discretization is not an M-matrix even for a self-adjoint PDE. Note also that for noninterface anisotropic problems with a constant matrix $\mathbf{A}$, we can apply a scaling transform to the original problem to get an isotropic one, which is not possible when $\mathbf{A}$ is a piecewise constant matrix with discontinuities. The problem becomes more challenging when the domain contains an arbitrary interface and nonhomogeneous jump conditions, that is, one or both of w and v are nonzero. In [9, 10], a first order accurate method was developed for elliptic anisotropic problems on irregular domains. A nine point stencil combining a linear optimization process is used so that the resulting linear system of equations is an M-matrix. A second order accurate kernel

free boundary integral method was applied to elliptic anisotropic PDEs on irregular domains [32]. An immersed finite element method (IFEM) with homogeneous jump conditions was presented in [1] that is second order accurate in $L^2(\Omega)$. The treatment of interface triangles is somewhat sophisticated in [1]. It is very difficult, if not impossible, to get a pointwise error estimate using IFEM. In [15, 16, 17], Petrov–Galerkin methods were developed in which the solution space is the immersed finite element (IFE) space while the test function space is the standard one. Numerical results reveal second order convergence in the infinity norm, which has not been proved theoretically yet except for some simple scalar cases such as for one-dimensional (1D) problems or two-dimensional (2D) problems with line interfaces that are parallel to coordinate axes [19].

In this paper, we propose a hybrid sharp interface method that combines the advantages of the finite element discretization for regular problems away from the interface and the maximum principle preserving immersed interface method at grid points near or on the interface. Note that an FEM can be regarded as a finite difference method using a structured mesh under some manipulations. In the new method, the resulting linear system of equations is composed of two parts: one is a semipositive definite part; the other part satisfies the conditions of an M-matrix. The jump conditions are enforced using the finite difference discretization. The linear system of equations is solved by the structured multigrid solver MGD9V [8]. We show that the new method is consistent with $O(h^2)$ local truncation errors at regular grid points if the P1 finite element is used while $O(h)$ is at irregular grid points near or on the interface. The global error is shown to be $O(h^2|\log h|)$ in the maximum norm by splitting the errors into three parts. We also propose a scaling technique along the interface to improve the condition of the continuous and discrete systems. Using a recently developed technique, we can compute the normal derivative or the gradient of the solution to second order accuracy except for a factor of $|\log h|$. Various numerical examples are presented to demonstrate the efficiency of the proposed method and convergence analysis. A mimic of a potential flow through an anisotropic object is also provided as a practical application.

The rest of this paper is organized as follows. In section 2, we present the finite element discretization based on a uniform triangular mesh at regular nodal (grid) points and carry out some analysis. In section 3, we describe the maximum principle preserving finite difference discretization at irregular grid points for the anisotropic interface problem. The section starts with some needed preparations, particularly the interface relations of the solution across the interface, followed by the construction of the finite difference discretization. Convergence analysis is presented in section 4. Furthermore, an immersed interface method (IIM) based interpolation scheme [27] is discussed to compute the normal derivative of the solution at the interface from each side of the interface. Numerical experiments are presented in section 5 along with an application example. We conclude in the last section.

2. The finite element/difference discretization at regular nodes. Let the domain Ω be a rectangular one, $\Omega = (a, b) \times (c, d)$. We use a unform triangulation,

$$x_i = a + ih, \quad 0, 1, \ldots, m; \quad y_j = c + jh, \quad j = 0, 1, \ldots, n. \tag{3}$$

For simplicity of presentation, we have assumed that $h = (b-a)/m = (d-c)/n$. The interface Γ is represented by the zero level set of a Lipschitz continuous function φ,

$$\Gamma = \Big\{ (x, y), \quad \varphi(x, y) = 0, \quad (x, y) \in \Omega \Big\}. \tag{4}$$

The level set representation is not unique and should be chosen close to the signed distance function from the interface. Thus, in the neighborhood of the interface, we can assume that $\varphi(x,y) \in C^2$ and $|\nabla\varphi| \sim 1$. In implementation, the level set function is defined at the grid points as φ_{ij} corresponding to $\varphi(x_i, y_j)$. At a grid point (x_i, y_j), we define

$$\begin{aligned} \varphi_{ij}^{\max} &= \max\left\{\varphi_{i-1,j}, \varphi_{ij}, \varphi_{i+1,j}, \varphi_{i,j-1}, \varphi_{i,j+1}, \varphi_{i+1,j-1}, \varphi_{i-1,j+1}\right\}, \\ \varphi_{ij}^{\min} &= \min\left\{\varphi_{i-1,j}, \varphi_{ij}, \varphi_{i+1,j}, \varphi_{i,j-1}, \varphi_{i,j+1}, \varphi_{i+1,j-1}, \varphi_{i-1,j+1}\right\}. \end{aligned} \tag{5}$$

A grid point (x_i, y_j) is called *regular* if $\varphi_{ij}^{\max}\varphi_{ij}^{\min} > 0$; otherwise it is called *irregular*. Our idea is to derive the finite difference scheme using a finite element discretization at regular grid points while using a maximum principle preserving finite difference scheme at irregular ones.

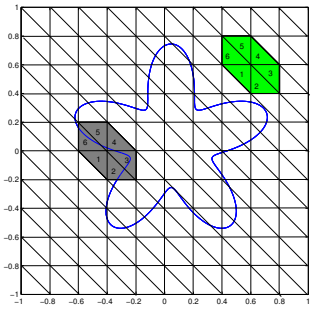

FIG. 2. *A uniform triangular mesh of a domain* Ω *containing a five-star interface* Γ. *The center of the six green triangles is a regular nodal (grid) point where an FE discretization is utilized, while the center of the six gray triangles is an irregular nodal (grid) point where a maximum preserving IIM is utilized. (Figure in color online.)*

We employ a finite element discretization at regular nodal points; see Figure 2 for an illustration. From the classical finite element theory and method (see, for example, [5, 7, 11]), we know that the solution $u(x,y) \in H^1(\Omega^{\pm})$ and the weak form of (1) is

$$a(u,v) = \int_\Omega fv\, d\mathbf{x} = L(v) \qquad \forall v \in H_0^1(\Omega^{\pm}), \tag{6}$$

where

$$\begin{aligned} a(u,v) &= \int_\Omega \left(\mathbf{A}\nabla u \cdot \nabla v + \sigma uv\right) d\mathbf{x} \\ &= \int_\Omega \left(A_{11}u_x v_x + A_{12}u_x v_y + A_{12}u_y v_x + A_{22}u_y v_y + \sigma uv\right)\, d\mathbf{x}. \end{aligned}$$

The solution space is also $H_0^1(\Omega^{\pm})$.

Let $V_h \subset H_0^1$ be the standard P_1 conforming finite element space associated with the uniform triangulation and $\{\psi_k\}_{k=1}^{N_{dof}}$ be a set of basis functions of V_h, where N_{dof} is the number of freedoms or unknowns. A finite element approximation to the original problem is

$$u_h(\mathbf{x}) = \sum_{k=1}^{N_{dof}} \alpha_k \psi_k(\mathbf{x}). \tag{7}$$

The linear system of equations for the unknowns $\{\alpha_k\}$ can be written as

$$A_h\mathbf{U} = \mathbf{F}, \qquad \mathbf{U} = \begin{bmatrix} \alpha_1 & \alpha_2 & \cdots & \cdots & \alpha_{N_{dof}} \end{bmatrix}^T, \tag{8}$$

where the matrix A_h is a symmetric positive definite (SPD) matrix whose elements are

$$a_{ij} = a(\psi_i, \psi_j) = \int_\Omega \Big(\mathbf{A}(\mathbf{x})\nabla\psi_i \cdot \nabla\psi_j + \sigma(\mathbf{x})\,\psi_i\psi_j \Big)\, d\mathbf{x} \quad \text{and}$$

$$F_i = \int_\Omega \psi_i f(\mathbf{x}) d\mathbf{x}. \tag{9}$$

The matrix A_h is block tridiagonal with at most seven nonzero entries in each row if the standard piecewise linear (tent) function $\psi_k(\mathbf{X}_l) = \delta_{kl}$ is used. Note that in this case we have $u_h(\mathbf{x}_k) = \alpha_k$, which is an approximate solution to the true solution $u(\mathbf{x}_k)$ at $\mathbf{x}_k$. Thus, the FEM can be regarded as a finite difference method since

$$A_h\mathbf{U} = \mathbf{F}, \qquad \mathbf{U} = \begin{bmatrix} U_1 & U_2 & \cdots & \cdots & U_{N_{dof}} \end{bmatrix}^T \tag{10}$$

if we define $\alpha_k = U_k \approx u(\mathbf{x}_k)$ as a finite difference approximation to the original problem.

If the matrix $\mathbf{A}$ is a constant matrix and σ is a constant, then we can compute entries of the coefficient matrix exactly since $\nabla\psi_i$ is a constant vector. Let $\triangle_e$ be a typical triangle element. Denote the nonzero P_1 basis functions on this element as ψ_1^e, ψ_2^e, and ψ_3^e. Then we have

$$\int_{\triangle_e} (\psi_1^e)^p (\psi_2^e)^q (\psi_3^e)^r dxdy = \frac{p!\,q!\,r!}{(p+q+r+2)!} 2|\triangle_e| \tag{11}$$

for integers p, q, and r; see, for example, [30]. Furthermore, let k be the index of the nodal points centered at $\mathbf{x}_k$. The load vector can be approximated by

$$F_k = \int_\Omega f(\mathbf{x})\,\psi_k(\mathbf{x})\,d\mathbf{x} \approx f_{ij} \int_\Omega \psi_k(\mathbf{x})\,d\mathbf{x} = h^2 f_{ij}, \tag{12}$$

where $f_{ij} = f(x_i, y_j) = f(\mathbf{x}_k)$. We approximate the entries of the mass matrix for the nodal point centered at $\mathbf{x}_k = (x_i, y_j)$ by

$$\int_\Omega \sigma(\mathbf{x})\psi_k(\mathbf{x})\psi_l(\mathbf{x})\,d\mathbf{x} \approx \delta_{kl}\,\sigma(\mathbf{x}_k)\,h^2 = \delta_{kl}\,\sigma_{ij}\,h^2,$$

which is derived from the following:

$$\int_e \sigma(\mathbf{x})\psi_k^e(\mathbf{x})\psi_l^e(\mathbf{x})\,d\mathbf{x} \approx \frac{|e|}{3}\sum_{m=1}^{3} \sigma(\mathbf{x}_m^e)\psi_k^e(\mathbf{x}_m^e)\psi_l^e(\mathbf{x}_m^e) = \frac{h^2}{6}\delta_{kl}\sigma(\mathbf{x}_k) = \frac{h^2}{6}\,\delta_{kl}\,\sigma_{ij}.$$

After some manipulations, we get the finite difference equation at (x_i, y_j) below,

$$\begin{aligned} &\frac{2(A_{11}+A_{12}+A_{22})U_{i,j}}{h^2} + \frac{A_{12}(U_{i+1,j-1}+U_{i-1,j+1})}{h^2} + \sigma_{ij}U_{ij} \\ &\quad - \frac{(A_{11}+A_{12})(U_{i-1,j}+U_{i+1,j}) + (A_{12}+A_{22})(U_{i,j-1}+U_{i,j+1})}{h^2} = f_{ij}. \end{aligned} \tag{13}$$

It is a seven-point stencil finite difference equation since the support of a basis function $\psi_k(\mathbf{x})$ defined on the nodal point $\mathbf{x}_k$ contains six elements. The following theorem states that the finite difference scheme is second order accurate in discretization in the infinity norm (pointwise) for noninterface problems.

THEOREM 1. *Assume that $u(x,y) \in C^4(\Omega)$, A and σ are constant in the entire domain Ω, $w = 0$, $v = 0$, $f(x,y) \in C(\Omega)$; then the finite difference scheme* (13) *has the following properties:*

1. *The finite difference scheme is a second order discretization to the PDE* (1)–(2)*, that is, the local truncation is bounded by Ch^2,*

$$|T_{ij}| \le C \max_{|\alpha|\le 4} |D^\alpha u|\, h^2, \tag{14}$$

where $D^\alpha u$ is defined as

$$D^\alpha u(\mathbf{x}) = \frac{\partial^{|\alpha|} u}{\partial x_1^{\alpha_1} \partial y^{\alpha_2}}, \quad |\alpha| = \alpha_1 + \alpha_2, \quad \alpha_i \ge 0, \quad i = 1, 2, \tag{15}$$

which is the multi-index notation for all partial derivatives.

2. *The finite difference solution has second order convergence in the infinity norm (pointwise) for noninterface problems, that is,*

$$\max_{ij} |u(x_i, y_j) - U_{ij}| \le \bar{C} |\log h| h^2, \tag{16}$$

where C and $\bar{C}$ depend on u, f, and $\{A_{ij}\}$.

Proof. The local truncation error at a grid point (x_i, y_j) is defined as

$$\begin{aligned} T_{ij} &= \tfrac{2(A_{11}+A_{12}+A_{22})u(x_i,y_j)}{h^2} + \tfrac{A_{12}(u(x_{i+1},y_{j-1})+u(x_{i-1},y_{j+1}))}{h^2} + \sigma(x_i,y_j)u(x_i,y_j) \\ &- \frac{(A_{11}+A_{12})(u(x_{i-1},y_j)+u(x_{i+1},y_j)) + (A_{12}+A_{22})(u(x_i,y_{j-1})+u(x_i,y_{j+1}))}{h^2} - f_{ij}. \end{aligned} \tag{17}$$

If we expand all $u(x_{i+i_k}, y_{j+j_k})$ in Taylor expansion at (x_i, y_j) using

$$\begin{aligned} u(x,y) = u_{ij} &+ (x-x_i)u_x + (y-y_j)u_y + \frac{1}{2}(x-x_i)^2 u_{xx} + (x-x_i)(y-y_j)u_{xy} \\ &+ \frac{1}{2}(y-y_j)^2 u_{yy} + \frac{1}{6}(x-x_i)^3 u_{xxx} + \frac{1}{2}(x-x_i)(y-y_j)^2 u_{xyy} \\ &+ \frac{1}{2}(x-x_i)^2(y-y_j)u_{xxy} + \frac{1}{6}(y-y_j)^3 u_{yyy} \\ &+ \frac{1}{24}\Big\{ (x-x_i)^4 u_{xxxx} + 4(x-x_i)(y-y_j)^3 u_{xyyy} + 6(x-x_i)^2(y-y_j)^2 u_{xxyy} \\ &+ 4(x-x_i)^3(y-y_j)u_{xxxy} + (y-y_j)^4 u_{yyyy} \Big\} + o(h^4), \end{aligned}$$

collect terms, and apply the PDE at (x_i, y_j), then we can arrive at

$$|T_{ij}| \le C \max_{|\alpha|\le 4} |D^\alpha u|\, h^2. \qquad \square$$

From classical FEM convergency analysis and Nitch's technique (see, for example, [6, 25]), we conclude that

$$\max_{ij} |u(x_i, y_j) - U_{ij}| \le C |\log h| h^2.$$

For variable matrix $\mathbf{A}(\mathbf{x})$, we use the following formula to approximate the matrix:

$$\mathbf{A}(\mathbf{x}) \approx \sum_k \mathbf{A}(\mathbf{x}_k)\psi_k(\mathbf{x}), \tag{18}$$

so that the integration can still be calculated accurately with $O(h^2)$ errors.

3. The maximum principle preserving finite difference scheme at irregular grid points. At irregular grid points, we use the maximum principle preserving scheme to discretize the PDE to get a sharp interface method that can provide an accurate solution at all grid points not just in average norms such as L^2 or H^1. The implementation is also simpler compared to the IFE [1] or the Petrov–Galerkin approach [16]. The idea and procedure are similar to the maximum principle preserving scheme [21] for scalar elliptic interface problems. But the technicality, theoretical analysis, and implementation are much more challenging as we can see from the discussions of this section and the error analysis later.

In the maximum principle preserving scheme, we mostly use the centered 9-point finite difference stencil except for a few cases as described later in this subsection. The finite difference equation at an irregular grid point (x_i, y_j) can be written as

$$\sum_{k=1}^{N_s} \gamma_{ij,k} U_{i+i_k, j+j_k} + \sigma_{ij} U_{ij} = f_{ij} + C_{ij}, \tag{19}$$

where i_k, j_k take values in the set $\{0, \pm 1, \pm 2, \ldots\}$, and C_{ij} is a correction term corresponding to the jump in the solution and the flux. The coefficients $\gamma_{ij,k}$ and the correction term C_{ij} are determined so that the local truncation error

$$T_{ij} = \sum_{k=1}^{N_s} \gamma_{ij,k} u(x_{i+i_k}, y_{j+j_k}) + \sigma(x_i, y_j) u(x_i, y_j) - f(x_i, y_j) - C_{ij} \tag{20}$$

can be as small as possible in terms of the magnitude. In the neighborhood of (x_i, y_j), the grid points involved are from different sides of the interface (Ω^- and Ω^+). Without of loss of generality, let us assume that $(x_i, y_j) \in \Omega^-$. The procedure to determine the finite difference coefficients and the correction term is as follows: We select a point (X_i^*, Y_j^*), often the orthogonal projection of (x_i, y_j) on the interface, expand all $u(x_{i+i_k}, y_{j+j_k})$ at (X_i^*, Y_j^*) from each side of the interface up to all second order partial derivatives, use interface relations to express the quantities from Ω^+ in terms of those from the Ω^- side, and finally collect terms to match the PDE at (X_i^*, Y_j^*) from the Ω^- side to get the linear system of equations for the coefficients and then the correction term. We refer the reader to [21] for details.

3.1. Interface relations for the anisotropic PDE. To set up the linear system of equations for the coefficients, it is necessary to express the quantities of the solution from one side in terms of those from the other side up to all the second order partial derivatives. Due to the anisotropy, the invariant assumption of the PDE and other quantities with the change of orthogonal coordinate systems is no longer true.

Let the normal direction at (X_i^*, Y_j^*) be $(\cos\theta^*, \sin\theta^*)$.[1] The local coordinate system in the neighborhood of (X_i^*, Y_j^*) is

$$\begin{cases} \xi = (x - X_i^*)\cos\theta^* + (y - Y_j^*)\sin\theta^*, \\ \eta = -(x - X_i^*)\sin\theta^* + (y - Y_j^*)\cos\theta^*, \end{cases} \tag{21}$$

where θ^* is the angle between the x-axis and the normal direction, pointing to the direction of a specified side, say the "+" side as illustrated in Figure 3. At a neighborhood of (X_i^*, Y_j^*) on the interface, the interface can be written as

$$\xi = \chi(\eta), \quad \text{with} \quad \chi(0) = 0, \quad \chi'(0) = 0. \tag{22}$$

[1] Some quantities in this subsection, such as θ^*, ξ_k, and η_k later depend on i and j. For simplicity of presentation, we omit the dependance.

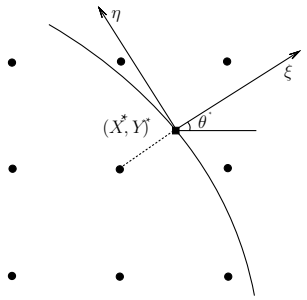

FIG. 3. *A local coordinate system and nearby grid points.*

Thus, we represent the interface Γ near (X_i^*, Y_j^*) using a new parametric form

$$\begin{cases} X(s) = X_i^* + \chi(s)\cos\theta^* - s\sin\theta^*, \\ Y(s) = Y_j^* + \chi(s)\sin\theta^* + s\cos\theta^*. \end{cases} \tag{23}$$

We have $(X(0), Y(0)) = (X^*, Y^*)$; here s can be regarded as arc-length parameter starting from (X^*, Y^*). The tangent vector then is

$$\begin{aligned} \boldsymbol{\tau}(s) &= \left[\frac{X'}{\sqrt{(X')^2 + (Y')^2}}, \frac{Y'}{\sqrt{(X')^2 + (Y')^2}}\right] \\ &= \left[\frac{\chi'\cos\theta^* - \sin\theta^*}{\sqrt{1 + (\chi')^2}}, \frac{\chi'\sin\theta^* + \cos\theta^*}{\sqrt{1 + (\chi')^2}}\right], \end{aligned} \tag{24}$$

with $\boldsymbol{\tau}(0) = [-\sin\theta^*, \cos\theta^*]$, and the normal direction is

$$\mathbf{n} = \left[\frac{\chi'\sin\theta^* + \cos\theta^*}{\sqrt{1 + (\chi')^2}}, \frac{-\chi'\cos\theta^* + \sin\theta^*}{\sqrt{1 + (\chi')^2}}\right]. \tag{25}$$

For simplicity, we still use the same notation for the solution u, $\mathbf{A}$, $[u] = w(s)$, and $[\mathbf{A}\nabla u \cdot \mathbf{n}] = v(s)$ in the local coordinate system. In the neighborhood of (X^*, Y^*), using the idea of the level set method, we can extend the quantities on the interface along the normal line using $\varphi(\xi, s) = \xi - \chi(s)$. Thus the tangential and normal derivatives and other interface quantities are also defined in the neighborhood as the normal extension of their value from the interface along the normal line.

To derive the jump relations and design the algorithm, we rewrite the governing equation (1) using the local coordinates as well to get

$$-(a_{11}u_{\xi\xi} + 2a_{12}u_{\xi\eta} + a_{22}u_{\eta\eta}) + \sigma u = f \tag{26}$$

after some efforts and manipulations, where

$$\begin{cases} a_{11} = A_{11}\cos^2\theta^* + A_{22}\sin^2\theta^* + 2A_{12}\cos\theta^*\sin\theta^*, \\ a_{22} = A_{11}\sin^2\theta^* + A_{22}\cos^2\theta^* - 2A_{12}\cos\theta^*\sin\theta^*, \\ a_{12} = (A_{22} - A_{11})\cos\theta^*\sin\theta^* + A_{12}(\cos^2\theta^* - \sin^2\theta^*). \end{cases} \tag{27}$$

Under the framework discussed above, we have the following theorem that states the interface relations needed for our algorithm design.

THEOREM 2. *If $u(x,y) \in C^2(\Omega^{\pm})$, $f(x,y) \in C(\Omega^{\pm})$, $\Gamma \in C^2$, $w \in C^2$, $v \in C^1$, then the following interface relations hold:*

$$
\begin{aligned}
u^+ &= u^- + w,\\
u^+_\xi &= \frac{a^-_{11}}{a^+_{11}}u^-_\xi - \frac{[a_{12}]}{a^+_{11}}u^-_\eta + \frac{1}{a^+_{11}}v - \frac{a^+_{12}}{a^+_{11}}w',\\
u^+_\eta &= u^-_\eta + w',\\
u^+_{\eta\eta} &= \chi''\frac{[a_{11}]}{a^+_{11}}u^-_\xi + \chi''\frac{[a_{12}]}{a^+_{11}}u^-_\eta + u^-_{\eta\eta} - \frac{\chi''}{a^+_{11}}v + \chi''\frac{a^+_{12}}{a^+_{11}}w' + w'',\\
u^+_{\xi\eta} &= \chi''\frac{a^+_{11}[a_{12}] - 2a^+_{12}[a_{11}]}{(a^+_{11})^2}u^-_\xi + \chi''\frac{a^+_{11}[a_{22}] - 2a^+_{12}[a_{12}]}{(a^+_{11})^2}u^-_\eta + \frac{a^-_{11}}{a^+_{11}}u^-_{\xi\eta}\\
&\quad - \frac{[a_{12}]}{a^+_{11}}u^-_{\eta\eta} + \chi''\frac{2a^+_{12}}{(a^+_{11})^2}v + \frac{1}{a^+_{11}}v' + \chi''\frac{(a^+_{11}a^+_{22} - 2(a^+_{12})^2)}{(a^+_{11})^2}w' - \frac{a^+_{12}}{a^+_{11}}w'',\\
u^+_{\xi\xi} &= -S_1\chi''u^-_\xi - S_2\chi''u^-_\eta + \frac{a^-_{11}}{a^+_{11}}u^-_{\xi\xi} + \frac{2a^+_{12}[a_{12}] - a^+_{11}[a_{22}]}{(a^+_{11})^2}u^-_{\eta\eta}\\
&\quad + \frac{2(a^+_{12}[a_{11}] - a^+_{11}[a_{12}])}{(a^+_{11})^2}u^-_{\xi\eta} - \frac{[f]}{a^+_{11}} + \frac{\sigma^+[u] + [\sigma]u^-}{a^+_{11}} + S_3,
\end{aligned}
\tag{28}
$$

where S_1, S_2, and S_3 are given as follows:

$$
\begin{aligned}
S_1 &= \frac{2a^+_{11}a^+_{12}[a_{12}] - 4(a^+_{12})^2[a_{11}] + a^+_{11}a^+_{22}[a_{11}]}{(a^+_{11})^3},\\
S_2 &= \frac{2a^+_{11}a^+_{12}[a_{22}] - 4(a^+_{12})^2[a_{12}] + a^+_{11}a^+_{22}[a_{12}]}{(a^+_{11})^3},\\
S_3 &= -\chi''\frac{4(a^+_{12})^2 - a^+_{11}a^+_{22}}{(a^+_{11})^3}v - \frac{2a^+_{12}}{(a^+_{11})^2}v'\\
&\quad - \chi''\frac{3a^+_{11}a^+_{12}a^+_{22} - 4(a^+_{12})^3}{(a^+_{11})^3}w' + \frac{2(a^+_{12})^2 - a^+_{11}a^+_{22}}{(a^+_{11})^2}w''.
\end{aligned}
\tag{29}
$$

Proof. Differentiating $[u] = w$ with respect to s once, we get

$$
[u_\xi]\,\chi' + [u_\eta] = w'(s). \tag{30}
$$

Differentiating the identity above with respect to s, we get

$$
[u_{\xi\xi}]\chi'^2 + 2[u_{\xi\eta}]\chi' + [u_\xi]\chi'' + [u_{\eta\eta}] = w''(s). \tag{31}
$$

Setting $s = 0$ in the above two identities and using $\chi'(0) = 0$, we obtain the third and the fourth identities in the theorem.

From $u_x = u_\xi\cos\theta^* - u_\eta\sin\theta^*$, $u_y = u_\xi\sin\theta^* + u_\eta\cos\theta^*$, and $\mathbf{n}(\mathbf{s})$ defined above, and the relation between A_{ij} and a_{ij}, and with some manipulations, we can rewrite

$[\mathbf{A}\nabla u \cdot \mathbf{n}]$ as

$$\begin{aligned}[\mathbf{A}\nabla u \cdot \mathbf{n}] &= \left[\begin{pmatrix} A_{11} & A_{12} \\ A_{12} & A_{22} \end{pmatrix} \begin{pmatrix} u_x \\ u_y \end{pmatrix} \cdot \begin{pmatrix} n_x \\ n_y \end{pmatrix} \right] \\ &= \left[\begin{pmatrix} A_{11}(u_\xi \cos\theta^* - u_\eta \sin\theta^*) + A_{12}(u_\xi \sin\theta^* + u_\eta \cos\theta^*) \\ A_{12}(u_\xi \cos\theta^* - u_\eta \sin\theta^*) + A_{22}(u_\xi \sin\theta^* + u_\eta \cos\theta^*) \end{pmatrix}^T \cdot \mathbf{n} \right] \\ &= \frac{1}{\sqrt{1+(\chi')^2}} \Big[\, (a_{11} - \chi' a_{12})\, u_\xi] + [(a_{12} - \chi' a_{22})\, u_\eta \Big].\end{aligned}$$

Therefore, the flux jump condition can be written as

$$\Big[\, (a_{11} - \chi' a_{12})\, u_\xi \Big] + \Big[\, (a_{12} - \chi' a_{22})\, u_\eta \Big] = \sqrt{1+(\chi')^2}\, v(s). \tag{32}$$

We get the second identity by setting $s = 0$.

To get the fifth identity, we differentiate the flux jump condition above with respect to s. The left-hand side then is

$$\begin{aligned}LHS = &\Big[\, (a_{11} - \chi' a_{12})\, (u_{\xi\xi}\chi' + u_{\xi\eta}) \Big] + \Big[\, -\chi'' a_{12} u_\xi \Big] \\ &+ \Big[\, (a_{12} - \chi' a_{22})\, (u_{\eta\xi}\chi' + u_{\eta\eta}) \Big] + \Big[\, -\chi'' a_{22} u_\eta \Big].\end{aligned}$$

The right-hand side is

$$RHS = \sqrt{1+(\chi')^2}\, v'(s) + \frac{\chi'\chi''}{\sqrt{1+(\chi')^2}}\, v(s).$$

By plugging $s = 0$ into the left- and right-hand sides and using $\chi'(0) = 0$, we get the fifth identity.

The last identity is obtained from the PDE using

$$-\left([a_{11}u_{\xi\xi}] + 2[a_{12}u_{\xi\eta}] + [a_{22}u_{\eta\eta}]\right) + [\sigma u] = [f]. \tag{33}$$

REMARK 1. *For variable coefficients $\mathbf{A}(\mathbf{x})$, $\sigma(\mathbf{x})$, and $f(\mathbf{x})$, the derivation process is similar, but the expressions are longer and more complicated. The PDE in the local coordinates is now*

$$-\left(a_{11}u_{\xi\xi} + 2a_{12}u_{\xi\eta} + a_{22}u_{\eta\eta} + c_1 u_\xi + c_2 u_\eta\right) + \sigma u = f, \tag{34}$$

where

$$c_1 = \frac{\partial a_{11}}{\partial \xi} + \frac{\partial a_{12}}{\partial \eta}, \qquad c_2 = \frac{\partial a_{12}}{\partial \xi} + \frac{\partial a_{22}}{\partial \eta}. \tag{35}$$

The first four identities are the same, and the last two are the following:

(36)

$$\begin{aligned}u^+_{\xi\eta} \;=\; & \frac{c_3^-[a_{11}] - a_{11}^-[c_3] - \chi'' a_{12}^+[a_{11}]}{(a_{11}^+)^2} u_\xi^- \\ & + \frac{c_3^+[a_{12}] - a_{11}^+[c_4] - \chi'' a_{12}^+[a_{12}]}{(a_{11}^+)^2} u_\eta^- - \frac{[a_{12}]}{a_{11}^+} u_{\eta\eta}^- \\ & + \frac{a_{11}^-}{a_{11}^+} u_{\xi\eta}^- + \frac{c_3^+ a_{12}^+ - a_{11}^+ c_4^+ - \chi''(a_{12}^+)^2}{(a_{11}^+)^2} w' - \frac{a_{12}^+}{a_{11}^+} w'' + \frac{\chi'' a_{12}^+ - c_3^+}{(a_{11}^+)^2} v + \frac{v'}{a_{11}^+},\end{aligned}$$

(37)
$$
\begin{aligned}
u^+_{\xi\xi} &= \frac{(a^+_{11})^2c^-_1 - a^+_{11}a^-_{11}c^+_1 - 2a^+_{12}(c^-_3[a_{11}] - a^-_{11}[c_3] - \chi''a^+_{12}[a_{11}]) - \chi''a^+_{11}a^+_{22}[a_{11}]}{(a^+_{11})^3}u^-_\xi \\
&+ \frac{a^+_{11}c^+_1[a_{12}] - (a^+_{11})^2[c_2] - 2a^+_{12}(c^+_3[a_{12}] - a^+_{11}[c_4] - \chi''a^+_{12}[a_{12}]) - \chi''a^+_{11}a^+_{22}[a_{12}]}{(a^+_{11})^3}u^-_\eta \\
&+ \frac{a^-_{11}}{a^+_{11}}u^-_{\xi\xi} + \frac{2a^+_{12}[a_{12}] - a^+_{11}[a_{22}]}{(a^+_{11})^2}u^-_{\eta\eta} + \frac{2(a^+_{12}[a_{11}] - a^+_{11}[a_{12}])}{(a^+_{11})^2}u^-_{\xi\eta} \\
&+ \frac{a^+_{11}a^+_{12}c^+_1 - (a^+_{11})^2c^+_2 - 2a^+_{12}(c^+_3a^+_{12} - a^+_{11}c^+_4 - \chi''(a^+_{12})^2) - \chi''a^+_{11}a^+_{12}a^+_{22}}{(a^+_{11})^3}w' \\
&+ \frac{2(a^+_{12})^2 - a^+_{11}a^+_{22}}{a^+_{11}}w'' + \frac{\chi''a^+_{11}a^+_{22} - a^+_{11}c^+_1 - 2a^+_{12}(\chi''a^+_{12} - c^+_3)}{(a^+_{11})^3}v - \frac{2a^+_{12}}{(a^+_{11})^2}v' \\
&+ \frac{\sigma^+[u] + [\sigma]u^-}{a^+_{11}} - \frac{[f]}{a^+_{11}},
\end{aligned}
$$

where c_k, $k = 1, 2, 3, 4$, are given below,

(38)
$$
\begin{aligned}
c_1 &= \frac{\partial a_{11}}{\partial \xi} + \frac{\partial a_{12}}{\partial \eta}, \quad c_2 = \frac{\partial a_{12}}{\partial \xi} + \frac{\partial a_{22}}{\partial \eta}, \\
c_3 &= \frac{\partial a_{11}}{\partial \eta} - \chi'' a_{12}, \quad c_4 = \frac{\partial a_{12}}{\partial \eta} - \chi'' a_{22}.
\end{aligned}
$$

3.2. Maximum principle preserving finite difference equations at irregular grid points. In this subsection, we explain how to find the finite difference coefficients $\gamma_{ij,k}'s$ and the correction term C_{ij}. This step involves setting up a linear system of equations with N_s (often $N_s = 9$) unknowns $\{\gamma_{ij,k}\}$ and six equations to match u, u_ξ, u_η, $u_{\xi\xi}$, $u_{\xi\eta}$, and $u_{\eta\eta}$, plus sign constraints. The constraint linear system of equations is solved at each irregular grid point by computers. The CPU time for this process is typically less than 5% of the total CPU time and decreases as the mesh gets finer.

To minimize the local truncation error in magnitude in (20), we expand each $u(x_{i+i_k}, y_{j+j_k})$ at (X^*_i, Y^*_j) under the local coordinates (21),

$$
u(x_{i+i_k}, y_{j+j_k}) = u^\pm + \xi_k u^\pm_\xi + \eta_k u^\pm_\eta + \frac{1}{2}\xi^2_k u^\pm_{\xi\xi} + \xi_k\eta_k u^\pm_{\xi\eta} + \frac{1}{2}\eta^2_k u^\pm_{\eta\eta} + O(h^3),
$$

where the "+" or "−" sign is chosen depending on whether (ξ_k, η_k) lies on the "+" or "−" side of Γ. In this way, the local truncation error T_{ij} can be written as

(39)
$$
\begin{aligned}
T_{ij} = {} & b_1u^- + b_2u^+ + b_3u^-_\xi + b_4u^+_\xi + b_5u^-_\eta + b_6u^+_\eta + b_7u^-_{\xi\xi} + b_8u^+_{\xi\xi} \\
& + b_9u^-_{\eta\eta} + b_{10}u^+_{\eta\eta} + b_{11}u^-_{\xi\eta} + b_{12}u^+_{\xi\eta} + \sigma^-u^- - f^- - C_{ij} + O(h),
\end{aligned}
$$

where the coefficients b_j's are defined below,

(40)
$$b_1 = \sum_{k\in K^-} \gamma_{ij,k}, \quad b_2 = \sum_{k\in K^+} \gamma_{ij,k}, \quad b_3 = \sum_{k\in K^-} \xi_k\gamma_{ij,k}, \quad b_4 = \sum_{k\in K^+} \xi_k\gamma_{ij,k},$$
$$b_5 = \sum_{k\in K^-} \eta_k\gamma_{ij,k}, \quad b_6 = \sum_{k\in K^+} \eta_k\gamma_{ij,k}, \quad b_7 = \frac{1}{2}\sum_{k\in K^-} \xi_k^2\gamma_{ij,k}, \quad b_8 = \frac{1}{2}\sum_{k\in K^+} \xi_k^2\gamma_{ij,k},$$
$$b_9 = \frac{1}{2}\sum_{k\in K^-} \eta_k^2\gamma_{ij,k}, \; b_{10} = \frac{1}{2}\sum_{k\in K^+} \eta_k^2\gamma_{ij,k}, \; b_{11} = \sum_{k\in K^-} \xi_k\eta_k\gamma_{ij,k}, \; b_{12} = \sum_{k\in K^+} \xi_k\eta_k\gamma_{ij,k}.$$

In the above expressions, the index sets K^+ and K^- are defined as

$$K^{\pm} = \Big\{ k : (\xi_k, \eta_k) \quad \text{is on the } \pm \text{ side of } \quad \Gamma \Big\}.$$

Using the interface relations (28) and $f_{ij} = f^- + O(h)$, we eliminate the quantities from the "+" side using those from the "−", and collect terms to get

(41)
$$\begin{aligned} T_{ij} \;=\; & B_1u^- + B_2u^-_\xi + B_3u^-_\eta + B_4u^-_{\xi\xi} + B_5u^-_{\eta\eta} + B_6u^-_{\xi\eta} + \sigma^-u^- - f^- \\ & + B_7 - C_{ij} + O(h), \end{aligned}$$

where

(42)
$$B_1 = b_1 + b_2 + b_8\frac{[\sigma]}{a^+_{11}},$$
$$B_2 = b_3 + b_4\frac{a^-_{11}}{a^+_{11}} - b_8\chi''\frac{2a^+_{11}a^+_{12}[a_{12}] - 4(a^+_{12})^2[a_{11}] + a^+_{11}a^+_{22}[a_{11}]}{(a^+_{11})^3} + b_{10}\chi''\frac{[a_{11}]}{a^+_{11}} + b_{12}\chi''\frac{a^+_{11}[a_{12}] - 2a^+_{12}[a_{11}]}{(a^+_{11})^2},$$
$$B_3 = b_5 - b_4\frac{[a_{12}]}{a^+_{11}} + b_6 - b_8\chi''\frac{2a^+_{11}a^+_{12}[a_{22}] - 4(a^+_{12})^2[a_{12}] + a^+_{11}a^+_{22}[a_{12}]}{(a^+_{11})^3} + b_{10}\chi''\frac{[a_{12}]}{a^+_{11}} + b_{12}\chi''\frac{a^+_{11}[a_{22}] - 2a^+_{12}[a_{12}]}{(a^+_{11})^2},$$
$$B_4 = b_7 + b_8\frac{a^-_{11}}{a^+_{11}} - a^-_{11},$$
$$B_5 = b_9 + b_{10} + b_8\frac{2a^+_{12}[a_{12}] - a^+_{11}[a_{22}]}{(a^+_{11})^2} - b_{12}\frac{[a_{12}]}{a^+_{11}} - a^-_{22},$$
$$B_6 = b_{11} + b_8\frac{2(a^+_{12}[a_{11}] - a^+_{11}[a_{12}])}{(a^+_{11})^2} + b_{12}\frac{a^-_{11}}{a^+_{11}} - 2a^-_{12},$$
$$\begin{aligned} B_7 = {} & \left(b_2 + b_8\frac{\sigma^+}{a^+_{11}}\right)w + \left\{-b_4\frac{a^+_{12}}{a^+_{11}} + b_6 - b_8\chi''\frac{3a^+_{11}a^+_{12}a^+_{22} - 4(a^+_{12})^3}{(a^+_{11})^3} + b_{10}\chi''\frac{a^+_{12}}{a^+_{11}} \right. \\ & \left. + b_{12}\frac{a^+_{11}a^+_{22} - 2(a^+_{12})^2}{(a^+_{11})^2}\chi''\right\}w' + \left\{b_8\frac{2(a^+_{12})^2 - a^+_{11}a^+_{22}}{(a^+_{11})^2} + b_{10} - b_{12}\frac{a^+_{12}}{a^+_{11}}\right\}w'' \\ & + \left\{b_4\frac{1}{a^+_{11}} - b_8\chi''\frac{4(a^+_{12})^2 - a^+_{11}a^+_{22}}{(a^+_{11})^3} - b_{10}\frac{\chi''}{a^+_{11}} + b_{12}\chi''\frac{2a^+_{12}}{(a^+_{11})^2}\right\}v \\ & + \left\{-b_8\frac{2a^+_{12}}{(a^+_{11})^2} + b_{12}\frac{1}{a^+_{11}}\right\}v' - b_8\frac{[f]}{a^+_{11}}. \end{aligned}$$

The system of equations for $\{\gamma_{ij,k}\}$'s is obtained by matching the PDE in (41) with (26) up to second partial derivative terms. Once we know $\{\gamma_{ij,k}\}$'s, then we set $C_{ij} = B_7$ so that $T_{ij} \sim O(h)$.

3.3. Enforcing the sign constraints and a scaling strategy. We hope that the finite difference scheme at irregular grid points is diagonally dominant and the coefficient matrix part has the property of an M-matrix. Thus, we impose the sign restrictions on the coefficients $\{\gamma_{ij,k}\}$'s in (19),

$$-\frac{C}{h^2} \le \gamma_{ij,k} \le 0 \quad \text{if} \quad (i_k, j_k) \neq (0,0), \quad 0 < \gamma_{ij,k} \le \frac{C}{h^2} \quad \text{if} \quad (i_k, j_k) = (0,0), \tag{43}$$

where C is a positive constant, along with the first six equations from (42). Such an equality and inequality system can be solved using a linear or quadratic optimization technique. There are quite a few available solvers. The one that we employed is the quadratic optimization solver in [24].

We start with the centered 9-point stencil and solve the optimization problem. If no feasible solution can be found, we add more grid points nearby until the optimization problem has a feasible solution. More than 9-centered grid points may be needed if the matrix is "bad conditioned"; see, for example, the left matrix $\mathbf{A}$ below,

$$\mathbf{A} = \begin{pmatrix} 1 & 5 \\ 5 & 100 \end{pmatrix}, \qquad \mathbf{B} = \begin{pmatrix} 20 & 5 \\ 5 & 19 \end{pmatrix}, \tag{44}$$

versus the "good conditioned" matrix $\mathbf{B}$ above.

Another way is to apply a preconditioning (scaling) strategy which works well. We can rescale the governing equations using a simple transformation. Let D_Γ be a diagonal matrix $D_\Gamma = \mathrm{diag}(d_1, d_2)$, $d_1 d_2 \neq 0$. We apply the following transform:

$$-\left(D_\Gamma^{-1}\nabla\right) \cdot \Big((D_\Gamma \mathbf{A}(\mathbf{x})) D_\Gamma \Big) \left(D_\Gamma^{-1}\nabla\right) u(\mathbf{x}) + \sigma(\mathbf{x}) u(\mathbf{x}) = f(\mathbf{x}), \quad \mathbf{x} \in \Omega^-, \tag{45}$$

to get a better conditioned PDE. If we define $\mathbf{y} = D_\Gamma \mathbf{x}$, then the new PDE is

$$-\nabla \cdot \left(\bar{\mathbf{A}} \nabla \bar{u}(\mathbf{y})\right) + \bar{\sigma}(\mathbf{y})\, \bar{u}(\mathbf{y}) = \bar{f}(\mathbf{y}), \tag{46}$$

with new variable $\mathbf{y}$, where $\bar{u}(\mathbf{y}) = \bar{u}(D_\Gamma \mathbf{x}) = u(\mathbf{x})$ and so on. We choose d_1 and d_2 such that the two diagonals are close to each other as much as possible. For example, we should choose $d_1 = 1$, $d_2 = 1/10$ for the matrix $\mathbf{A}$ in the example above. The transform is to set the scaling $y_1 = x_1$, $y_2 = x_2/10$ to get the new PDE and the scaled domain. With the scaling, the 9-centered grid points stencil is enough for all our testing problems.

Note that it is enough just to scale the anisotropic matrix $\mathbf{A}$ near the interface while the transformation is on the entire domain. Since the transformed problem is still self-adjoint, the discrete matrix part of the finite difference scheme derived from the finite element discretization is still symmetric positive definite.

4. Convergence analysis for the finite element-finite difference (FE-FD) method. We first state the main convergence result.

THEOREM 3. *Let $u(x,y) \in C^4(\Omega^\pm)$ be the solution of (1)–(2). Assume that $\partial\Omega$ is Lipschitz continuous, and the interface is smooth ($C^2(s)$), $A(\mathbf{x})$ is a piecewise constant symmetric positive definite matrix, $\sigma(\mathbf{x})$ is a piecewise constant, and the*

finite difference coefficients $\{\gamma_{ij,k}\}$ *at irregular grid points satisfy*[2]

$$\sum_{\xi_k \geq 0} \gamma_{ij,k}\xi_k \geq \frac{C_2}{h}. \tag{47}$$

Then we have the following error estimate for the computed solution U_{ij} *of the FE-FD method with regular* $P1$ *finite element at regular grid points and the maximum principle preserving FD scheme at irregular grids points:*

$$\max_{ij} |u(x_i, y_j) - U_{ij}| \leq C|\log h|\, h^2, \tag{48}$$

where C *is an* $O(1)$ *quantity that depends on the underlined grid, interface,* u*,* f*, and* a_{ij}*. That is, the method is second order accurate in pointwise norm.*

Proof. Let the coefficient matrix of the finite difference scheme be $\mathbf{B}_h$, and the error vector of the computed finite difference solution be $\mathbf{E}_h$; then we have

$$\mathbf{B}_h\mathbf{E}_h = \mathbf{T}_h = \mathbf{T}_h^+ + \mathbf{T}_h^\Gamma + \mathbf{T}_h^-, \tag{49}$$

where entries of $\mathbf{T}_h^+$ are the local truncation errors of the finite difference scheme at regular grid points in Ω^+, and are zeros at regular grid points in Ω^-, and irregular grid points in the neighborhood of Γ and so on.

We define $\mathbf{B}_h^+$ as the finite difference (from FEM) operator on the entire domain with the anisotropic matrix $\mathbf{A}^+$ defined on Ω^+, that is, extended to the entire domain since $\mathbf{A}^+$ is a constant matrix. $\mathbf{B}_h^-$ is defined in the same way. $\mathbf{B}_h^+$ and $\mathbf{B}_h^-$ are symmetric positive definite matrices. Note also that since $\mathbf{A}$ is a piecewise constant matrix, the coefficient matrices $\mathbf{B}_h^+$ and $\mathbf{B}_h^-$ are exact due to the formulas in (11). The error in approximating the load vector is of $O(h^2)$ which has the same order as the local truncation errors. Finally, we define $\mathbf{B}_h^\Gamma$ as an extension of the maximum preserving finite difference scheme at irregular grid points to all grid points. $\mathbf{B}_h^\Gamma$ should be second order accurate at regular grid points and at an M-matrix if it would be applied to a noninterface problem. Note that the extension is used for the theoretical purpose but not for the computational practice since it would be computationally expensive.

If we define $\mathbf{E}_h^+$, $\mathbf{E}_h^-$, and $\mathbf{E}_h^\Gamma$ in the same way as their counterparts by replacing $\mathbf{T}$ with $\mathbf{E}$, then

$$\mathbf{E}_h = \mathbf{E}_h^+ + \mathbf{E}_h^\Gamma + \mathbf{E}_h^- = \left(\mathbf{B}_h^+\right)^{-1}\mathbf{T}_h^+ + \left(\mathbf{B}_h^\Gamma\right)^{-1}\mathbf{T}_h^\Gamma + \left(\mathbf{B}_h^-\right)^{-1}\mathbf{T}_h^-. \tag{50}$$

We show below that each term on the right-hand side is bounded by $O(h^2)$ or $O(|\log h|h^2)$.

The first term corresponds to the error estimate of the following problem:

$$-\nabla\cdot\left(\mathbf{A}^+(\mathbf{x})\nabla q(\mathbf{x})\right) + \sigma^+(\mathbf{x})q(\mathbf{x}) = \begin{cases} T_f^+(\mathbf{x}) & \text{if } \mathbf{x}\in\Omega^+, \\ 0 & \text{otherwise,} \end{cases} \qquad q\Big|_{\partial\Omega} = 0,$$

where

$$T_f^+(\mathbf{x}) = \sum_{\mathbf{x}_k\in\Omega^+} T_k\,\psi_k(\mathbf{x}), \qquad \text{and thus} \qquad \|T_f^+\|_{L^\infty} \leq Ch^2,$$

[2]This is a consistent condition in approximating the flux jump condition.

and T_k is the local truncation error at a regular nodal point $\mathbf{x}_k$ in (17). Note that this is an anisotropic elliptic problem with smooth coefficients but a source term with a finite discontinuity.

We claim that $q \in W^{2,\infty}(\Omega)$. As a matter of fact, $q(\mathbf{x})$ is piecewise smooth (see, for example, [2]). In particular,

$$q(\mathbf{x})|_{\Omega^\pm} \in C^2(\bar{\Omega}^\pm).$$

Define $p(\mathbf{x})$ by

$$p(\mathbf{x})|_{\Omega^\pm} = \left(q(\mathbf{x})|_{\Omega^\pm}\right)_{xx}.$$

Then $p(\mathbf{x}) \in L^\infty(\Omega)$. It can be shown in the following that $p(\mathbf{x})$ is the weak second derivative of $q(\mathbf{x})$ with respect to x. For any $\varphi \in C_0^\infty(\Omega)$,

$$\begin{aligned}\int_\Omega p\varphi \, d\mathbf{x} &= \sum_{i=1}^{2} \int_{\Omega_i} q_{xx}\varphi \, d\mathbf{x} = -\sum_{i=1}^{2} \left(\int_{\Omega_i} q_x \varphi_x \, d\mathbf{x} - \int_{\partial\Omega_i} q_x \varphi n_x \, ds \right) \\ &= -\sum_{i=1}^{2} \left(-\int_{\Omega_i} q\varphi_{xx} \, d\mathbf{x} + \int_{\partial\Omega_i} q\varphi_x n_x ds - \int_{\partial\Omega_i} q_x \varphi n_x \, ds \right) \\ &= \int_\Omega q\varphi_{xx} \, d\mathbf{x} + \int_\Gamma \left(-[q\varphi_x n_x^\Gamma] + [q_x \varphi n_x^\Gamma] \right) ds = \int_\Omega q\varphi_{xx} \, d\mathbf{x},\end{aligned}$$

where $\Omega_1 = \Omega^+$, $\Omega_2 = \Omega^-$, (n_x, n_y) is the normal direction of $\partial\Omega$, (n_x^Γ, n_y^Γ) is the normal direction of Γ, and we have used $q(\mathbf{x}) \in C^1(\bar{\Omega})$ to derive the last identity. Therefore, $q_{xx} = p \in L^\infty(\Omega)$. Similarly, $q_{xy}, q_{yy} \in L^\infty(\Omega)$. As a consequence, $q \in W^{2,\infty}(\Omega)$. Thus, the finite element discretization using P_1 element satisfies the following estimate from [25]:

$$\|\mathbf{E}_h^+\|_\infty \le C|\log h| \|q\|_{W^{2,\infty}(\Omega)} \le Ch^2 |\log h| \|u\|_{W^{2,\infty}(\Omega)}.$$

We can get the same order estimate for $\|\mathbf{E}_h^-\|_\infty$. The proof of above was due to Wu [31].

Finally, we prove the error estimate for $\mathbf{E}_h^\Gamma$. The proof is similar to the maximum preserving IIM [21] for the scalar case. Consider the solution to the following interface problem:

$$\begin{aligned} -\nabla \cdot (\mathbf{A}\nabla\phi(\mathbf{x})) + \sigma\phi(\mathbf{x}) &= 1, \\ [\phi] = 0, \qquad [\mathbf{A}\nabla\phi \cdot \mathbf{n}] &= 1, \quad \phi_{\partial\Omega} = 1. \end{aligned} \tag{51}$$

From the results in [2], we know that the solution ϕ exists, and it is unique and piecewise smooth. Therefore, the solution is also bounded. Let

$$\bar{\phi}(x,y) = \phi(x,y) + \left| \min_{(x,y)\in\Omega} \phi(x,y) \right|. \tag{52}$$

Note that the second term on the right-hand side is a constant. If (47) is true, then we know that

$$\mathbf{B}_h^\Gamma \bar{\phi}(x_i, y_j) \ge \begin{cases} 1 + O(h^2) & \text{if } (x_i, y_j) \text{ is a regular grid point,} \\ \displaystyle\sum_{\xi_k \ge 0} \gamma_k \xi_k \ge \frac{C_2}{h} + O(1) & \text{if } (x_i, y_j) \text{ is an irregular grid point.} \end{cases}$$

Note that the second inequality above is due to the jump in the flux in $\bar{\phi}$ at irregular grid points; and $\mathbf{B}_h^\Gamma \bar{\phi}(x_i, y_j)$ can be very large even though it is nonnegative. At regular grid points we have

$$\frac{|T_{ij}|}{\mathbf{B}_h^\Gamma \bar{\phi}(x_i, y_j)} \le \frac{C_3 h^2}{1},$$

where T_{ij} is the local truncation error if we would apply $\mathbf{B}_h^\Gamma$ to the original PDE at a regular grid point $\mathbf{x}_k = (x_i, y_j)$. At irregular grid points where (47) is satisfied, we have

$$\frac{|T_{ij}|}{\mathbf{B}_h^\Gamma \bar{\phi}(x_i, y_j)} \le \frac{C_4 h}{C_2/h} = \frac{C_4}{C_2} h^2,$$

since the local truncation errors at irregular grid points are bounded by

$$|T_{ij}| \le C_4 h$$

for some constant C_4. Thus, from Theorem 6.2 in [23], we also have $\|\mathbf{E}_h^\Gamma\|_\infty \le Ch^2$. This completes the proof.

REMARK 2. *We believe that the convergence theorem is also true for variable coefficient matrix* $\mathbf{A}$ *at least asymptotically. This is because at regular grid points, the differences of the computed coefficient matrix* $\mathbf{A}_h$ *and the exact one using the* P_1 *FEM is of order* $O(h^2)$.

4.1. Obtain approximate normal derivatives for the anisotropic interface problem. If needed, we can also obtain nearly second order accurate first order partial derivatives at any point in the domain using an IIM type interpolation [27]. We briefly explain how to compute the normal derivatives of the solution at points (X^*, Y^*) on the interface from each side of the interface. The key is to use a least squares interpolation and take into account the jump relations.

The normal derivatives of the solution at a point (X^*, Y^*) on the interface from the Ω^- side can be approximated by

$$\left.\frac{\partial U^-}{\partial n}\right|_{(X^*,Y^*)} \approx \sum_{k=1}^{\overline{N}_s} \overline{\gamma}_{i+i_k,j+j_k} U_{i+i_k,j+j_k} - \overline{C}, \tag{53}$$

where $\overline{N}_s$ is the number of grid points used in the interpolation and is often chosen between $9 \sim 12$ and the point (x_i, y_j) is the closest grid point to (X^*, Y^*). The coefficients $\overline{\gamma}_{i+i_k,j+j_k}$ are chosen so that the error of the interpolation can be minimized in the magnitude,

$$T^D = \sum_{k=1}^{\overline{N}_s} \overline{\gamma}_{i+i_k,j+j_k} u(x_{i+i_k}, y_{j+j_k}) - \overline{C} - \frac{\partial u^-}{\partial n}(X^*, Y^*). \tag{54}$$

The procedure to determine the coefficients $\overline{\gamma}_{i+i_k,j+j_k}$ and the correction term $\overline{C}$ is almost the same as that of C_{ij} in section 3.2 except that the number of grid points is different, as is the size of the linear system of equations; the right-hand side of the linear system of equations is now $\begin{bmatrix} 0 & 1 & 0 & 0 & 0 & 0 \end{bmatrix}^T$.

It has been shown in [27] that the computed normal derivative is second order accurate except for a factor of $\log h$ which has been confirmed in our numerical results in the next section.

5. Numerical experiments and analysis. We present several typical examples to show that the new finite difference method works well as analyzed. The finite difference equations are solved using the multigrid method DMGD9V [8]. We present two error measurements

$$\|E_N\|_\infty = \max_{ij} |u(x_i, y_j) - U_{ij}| \text{ and } \|E_D^\pm\|_\infty = \max_{1\le k\le N_b} \left| \frac{\partial u}{\partial n}^{\pm}(X_k^*, Y_k^*) - \frac{\partial U_k}{\partial n}^{\pm} \right|, \tag{55}$$

where N is the number of grid lines in the x- and y-directions and N_b is the number of points on the interface corresponding to all irregular grid points. We use the following formula to estimate convergence orders:

$$\text{order} = \left| \frac{\log(\|E_{N_1}\|_\infty / \|E_{N_2}\|_\infty)}{\log(N_1/N_2)} \right|, \tag{56}$$

with two different N's.

Example 5.1. We start with an example in which the anisotropic coefficient matrix $\mathbf{A}$ is a piecewise constant matrix. Note that, in general, we cannot use a scaling transform to change the problem to an isotropic interface problem. Since our method allows discontinuities for $f(x, y)$ and nonhomogeneous jump conditions, given a domain and an interface, and $\mathbf{A}$ and $\sigma(x, y)$, we can select almost any piecewise smooth solution first, then determine the source term f, and the jump conditions $[u]$ and $[\mathbf{A}\nabla u \cdot \mathbf{n}]$. We designate the solution as

$$u(x, y) = \begin{cases} x^2 - y^2 & \text{if } x^2 + 4y^2 \le 1, \\ \sin x \cos y & \text{if } x^2 + 4y^2 > 1. \end{cases} \tag{57}$$

We select the domain as $-2 \le x, y \le 2$, and the interface is an ellipse $x^2 + 4y^2 = 1$, and Ω^- is the domain inside the ellipse.

In Tables 1–4, we show grid refinement results to get actual errors in the strongest norm and average convergence order for various $\mathbf{A}^+$ and $\mathbf{A}^-$. In these tables, the first column is the mesh size in both x- and y- directions, the second column is the infinity error of the computed solution and the computed convergence order on the right, and the third and fourth columns are the errors and convergence order of the normal derivative of the solution at the interface from the Ω^- and Ω^+ sides, respectively. In the last row, we list the average of the convergence order of the three error measurements. Tables 1–2 show the results with modest jump in the coefficient matrix and σ, while there are large jump ratios in Tables 3–4. In all of the cases, we see a clean second order convergence in the solution and nearly second order convergence in the normal derivative.

Example 5.2. In this example, we use a more general interface that is both concave and convex. The interface Γ is given as follows:

$$\begin{cases} X = \Big(r_0 + \epsilon \sin(\omega\theta) \Big) \cos\theta + x_c, \\ Y = \Big(r_0 + \epsilon \sin(\omega\theta) \Big) \sin\theta + y_c, \end{cases} \qquad 0 \le \theta < 2\pi, \tag{58}$$

with the domain $[-1,\ 1]^2$. The domain contains (x_c, y_c) is denoted as Ω^-. The true solution is designated as

$$u(x, y) = \begin{cases} r^2 & \text{if } (x, y) \in \Omega^-, \\ r^4 + C_0 \log(2r) & \text{if } (x, y) \in \Omega^+, \end{cases} \tag{59}$$

TABLE 1

A grid refinement analysis of the new FD method for Example 5.1 *with* $\max_{i,j}\{|\ A_{ij}^{+}\ |\ /\ |\ A_{ij}^{-}\ |\} = 15$, $\sigma^{+}/\sigma^{-} = 10$.

N	$A^{-} = \begin{pmatrix} 4 & 2 \\ 2 & 5 \end{pmatrix}$, $A^{+} = \begin{pmatrix} 40 & 30 \\ 30 & 60 \end{pmatrix}$, $\sigma^{-} = 1, \sigma^{+} = 10$					
	$\|E\|_\infty$	Order	$\|E_D^{-}\|_\infty$	Order	$\|E_D^{+}\|_\infty$	Order
34	2.0945E-02		2.2665E-01		3.1829E-02	
66	5.8796E-03	1.92	3.0195E-02	3.04	9.8208E-03	1.77
130	1.3855E-03	2.13	7.6558E-03	2.02	2.9231E-03	1.79
258	3.3183E-04	2.09	2.2817E-03	1.77	7.2017E-04	2.04
514	8.5038E-05	1.98	5.8401E-04	1.98	1.8004E-04	2.01
Average		2.03		2.20		1.90

TABLE 2

A grid refinement analysis of the new FD method for Example 5.1 *with* $\max_{i,j}\{|\ A_{ij}^{+}\ |\ /\ |\ A_{ij}^{-}\ |\} = 1/15$, $\sigma^{+}/\sigma^{-} = 1/10$.

N	$A^{-} = \begin{pmatrix} 40 & 30 \\ 30 & 60 \end{pmatrix}$, $A^{+} = \begin{pmatrix} 4 & 2 \\ 2 & 5 \end{pmatrix}$, $\sigma^{-} = 10, \sigma^{+} = 1$					
	$\|E\|_\infty$	Order	$\|E_D^{-}\|_\infty$	Order	$\|E_D^{+}\|_\infty$	Order
34	1.3549E-02		3.1903E-02		9.0133E-02	
66	2.4122E-03	2.60	3.7644E-03	3.22	1.2859E-02	2.94
130	7.2843E-04	1.77	9.8295E-04	1.98	3.4296E-03	1.95
258	1.5315E-04	2.28	3.1457E-04	1.66	9.0853E-04	1.94
514	3.9274E-05	1.97	9.1841E-05	1.79	2.6389E-04	1.79
Average		2.15		2.16		2.15

TABLE 3

A grid refinement analysis of the new FD method for Example 5.1 *with* $\max_{i,j}\{|\ A_{ij}^{+}\ |\ /\ |\ A_{ij}^{-}\ |\} = 2000$, $\sigma^{+}/\sigma^{-} = 1000$.

N	$A^{-} = \begin{pmatrix} 0.2 & 0.05 \\ 0.05 & 0.4 \end{pmatrix}$, $A^{+} = \begin{pmatrix} 400 & 100 \\ 100 & 500 \end{pmatrix}$, $\sigma^{-} = 0.05, \sigma^{+} = 50$					
	$\|E\|_\infty$	Order	$\|E_D^{-}\|_\infty$	Order	$\|E_D^{+}\|_\infty$	Order
34	1.4830E-02		4.7553E+00		2.4329E-02	
66	4.5473E-03	1.78	1.0244E+00	2.31	7.9998E-03	1.68
130	1.0505E-03	2.16	2.5469E-01	2.05	2.2407E-03	1.88
258	2.4062E-04	2.15	7.4826E-02	1.79	5.4427E-04	2.06
514	6.2546E-05	1.95	2.8610E-02	1.39	1.4839E-04	1.89
Average		2.01		1.89		1.88

TABLE 4

A grid refinement analysis of the new FD method for Example 5.1 *with* $\max_{i,j}\{|\ A_{ij}^{+}\ |\ /\ |\ A_{ij}^{-}\ |\} = 1/1000$, $\sigma^{+}/\sigma^{-} = 1/1000$.

N	$A^{-} = \begin{pmatrix} 100 & 10 \\ 10 & 200 \end{pmatrix}$, $A^{+} = \begin{pmatrix} 0.1 & 0.01 \\ 0.01 & 0.2 \end{pmatrix}$, $\sigma^{-} = 10, \sigma^{+} = 0.01$					
	$\|E\|_\infty$	Order	$\|E_D^{-}\|_\infty$	Order	$\|E_D^{+}\|_\infty$	Order
34	2.2388E-02		6.3711E-02		2.4952E+00	
66	6.6879E-03	1.82	2.3155E-02	1.53	3.5806E-01	2.93
130	7.4593E-04	3.24	7.0894E-03	1.75	1.3412E-01	1.45
258	1.6719E-04	2.18	3.1358E-03	1.19	5.0391E-02	1.43
514	2.4733E-05	2.77	4.9010E-04	2.69	1.0795E-02	2.24
Average		2.50		1.79		2.01

where $r = \sqrt{x^2 + y^2}$.

In Tables 5–7, we show grid refinement results for Example 5.2. Tables 5–6 show the results with modest jump in the coefficient matrix and σ, while there are large jump ratios in Table 7. In all of the cases, we see a clean second order convergence in the solution and nearly second order convergence in the normal derivative.

TABLE 5

A grid refinement analysis of the new FD method for Example 5.2 *with* $\max_{i,j}\{|\ A_{ij}^+\ |\ /\ |\ A_{ij}^-\ |\} = 20$, $\sigma^+/\sigma^- = 10$.

N	$A^- = \begin{pmatrix} 3 & -1 \\ -1 & 5 \end{pmatrix}$, $A^+ = \begin{pmatrix} 40 & -20 \\ -20 & 60 \end{pmatrix}$, $\sigma^- = 1, \sigma^+ = 10$					
	$\|E\|_\infty$	Order	$\|E_D^-\|_\infty$	Order	$\|E_D^+\|_\infty$	Order
34	4.6988E-02		1.3270E+00		2.7143E-01	
66	9.6894E-03	2.38	5.2154E-01	1.41	1.4334E-01	0.96
130	1.2014E-03	3.08	1.5331E-01	1.81	2.7026E-02	2.46
258	3.6719E-04	1.73	1.8017E-02	3.12	4.6702E-03	2.56
514	9.9518E-05	1.89	2.2512E-03	3.02	4.7853E-04	3.31
Average		2.27		2.34		2.32

TABLE 6

A grid refinement analysis of the new FD method for Example 5.2 *with* $\max_{i,j}\{|\ A_{ij}^+\ |\ /\ |\ A_{ij}^-\ |\} = 1/20$, $\sigma^+/\sigma^- = 1/10$.

N	$A^- = \begin{pmatrix} 40 & -20 \\ -20 & 60 \end{pmatrix}$, $A^+ = \begin{pmatrix} 3 & -1 \\ -1 & 5 \end{pmatrix}$, $\sigma^- = 10, \sigma^+ = 1$					
	$\|E\|_\infty$	Order	$\|E_D^-\|_\infty$	Order	$\|E_D^+\|_\infty$	Order
34	7.7291E-02		6.0733E-01		1.6652E+00	
66	1.2565E-02	2.74	2.7770E-01	1.18	1.4635E+00	0.19
130	5.7518E-04	4.55	4.2952E-02	2.75	1.8548E-01	3.05
258	1.6144E-04	1.85	6.5318E-03	2.75	1.8440E-02	3.37
514	3.5404E-05	2.20	6.8731E-04	3.27	2.6709E-03	2.80
Average		2.84		2.49		2.35

TABLE 7

A grid refinement analysis of the new FD method for Example 5.2 *with* $\max_{i,j}\{|\ A_{ij}^+\ |\ /\ |\ A_{ij}^-\ |\} = 4000$, $\sigma^+/\sigma^- = 1000$.

N	$A^- = \begin{pmatrix} 0.1 & 0.02 \\ 0.02 & 0.2 \end{pmatrix}$, $A^+ = \begin{pmatrix} 400 & 20 \\ 20 & 500 \end{pmatrix}$, $\sigma^- = 0.1, \sigma^+ = 100$					
	$\|E\|_\infty$	Order	$\|E_D^-\|_\infty$	Order	$\|E_D^+\|_\infty$	Order
34	5.5350E-02		6.9755E+01		2.7100E-01	
66	1.1551E-02	2.36	3.9579E+00	4.33	8.4613E-02	1.75
130	1.2535E-03	3.28	1.3206E+00	1.62	1.0681E-02	3.05
258	4.2986E-04	1.56	4.3588E-01	1.62	1.5241E-03	2.84
514	1.0350E-04	2.07	2.6865E-01	0.70	3.8291E-04	2.00
Average		2.32		2.07		2.41

Example 5.3. In this example, the anisotropic coefficient of the PDE is a piecewise variable function,

$$\mathbf{A}^-(x,y) = \begin{pmatrix} x^2+y^2+1 & x^2+y^2 \\ x^2+y^2 & x^2+y^2+2 \end{pmatrix}, \quad \mathbf{A}^+ = \beta \mathbf{A}^-. \tag{60}$$

The $\sigma(\mathbf{x})$ term is also a piecewise variable function,

$$\sigma^-(x,y) = e^x \left(x^2+y^2+3\right) \sin y, \qquad \sigma^+(x,y) = \beta \sigma^-(x,y).$$

The designated true solution is

$$u(x,y) = \begin{cases} e^x \cos y & \text{if } x^2+y^2 \le r_0^2, \\ x^2+y^2 & \text{if } x^2+y^2 > r_0^2. \end{cases} \tag{61}$$

The domain is selected as $-1 \le x, y \le 1$, the interface is a circle $\sqrt{x^2+y^2} = r_0$, and Ω^- is the domain inside the circle. The source term can be derived from the governing equation as

$$f(x,y) = \begin{cases} 2e^x \left(\left(x+y-\dfrac{1}{2} \right) \cos y - (x^2+y^2+x+y) \sin y \right) + \sigma^- u^- & \text{if } x^2+y^2 \le r_0^2, \\ 8\beta \left(x^2+y^2+xy+\dfrac{3}{4} \right) + \sigma^+ u^+ & \text{if } x^2+y^2 > r_0^2. \end{cases} \tag{62}$$

The boundary and jump conditions can also be derived from the set-up, for example,

$$\begin{aligned} [\mathbf{A}(\mathbf{x}) \nabla u \cdot \mathbf{n}] = {} & 2\beta \Big\{ (X+Y)(X^2+Y^2) + X \Big\} \cos\theta \\ & + 2\beta \Big\{ (X+Y)(X^2+Y^2) + 2Y \Big\} \sin\theta \\ & - e^X \Big\{ (X^2+Y^2+1) \cos Y - (X^2+Y^2) \sin Y \Big\} \cos\theta \\ & - e^X \Big\{ (X^2+Y^2) \cos Y - (X^2+Y^2+2) \sin Y \Big\} \sin\theta, \end{aligned}$$

where $\mathbf{n} = (\cos\theta, \sin\theta) = (X,Y)/\sqrt{X^2+Y^2}$ on the interface.

TABLE 8
A grid refinement analysis of the new FD method for Example 5.3 *with* $\beta = 2$.

N	$\beta = 2$					
	$\|E\|_\infty$	Order	$\|E_D^-\|_\infty$	Order	$\|E_D^+\|_\infty$	Order
34	5.8805E-03		1.8585E-02		1.0555E-02	
66	1.3311E-03	2.24	3.3591E-03	2.58	1.8873E-03	2.60
130	3.0643E-04	2.17	1.1494E-03	1.58	6.7188E-04	1.52
258	7.6114E-05	2.03	2.6276E-04	2.14	1.6726E-04	2.03
514	1.9675E-05	1.96	8.4371E-05	1.65	4.5014E-05	1.90
Average		2.10		1.99		2.01

In Tables 8–9, we show grid refinement results for two typical β. The larger β means larger jumps. Once again, we observe second order convergence for both the solution and the normal derivative.

TABLE 9
A grid refinement analysis of the new FD method for Example 5.3 *with* $\beta = 1000$.

N	$\beta = 1000$					
	$\|E\|_\infty$	Order	$\|E_D^-\|_\infty$	Order	$\|E_D^+\|_\infty$	Order
34	6.5024E-03		2.0607E+00		1.3746E-02	
66	1.4451E-03	2.27	5.0159E-01	2.13	2.4304E-03	2.61
130	3.2462E-04	2.20	1.6819E-01	1.62	7.4474E-04	1.75
258	8.0086E-05	2.04	3.2572E-02	2.40	2.5055E-04	1.60
514	2.0913E-05	1.95	1.1286E-02	1.54	6.3751E-05	1.99
Average		2.12		1.92		1.99

Example 5.4. As suggested by one of the referees, we compared our method with other Cartesian mesh methods for anisotropic elliptic interface problems.

We first compare the results with the Petrov–Galerkin method [29] in which

$$\mathbf{A}^-(x,y) = \begin{pmatrix} x^2+3 & \cos(x) \\ \cos(x) & y^2+2 \end{pmatrix}, \quad \mathbf{A}^+ = 1000\mathbf{A}^-, \qquad \Omega = [-1,\ 1]^2, \tag{63}$$

with $\sigma = 0$, and the analytic solution

$$u(x,y) = \begin{cases} \sin(10xy) & \text{if } x^2+y^2 \le 0.15, \\ \sin(5xy)+1 & \text{if } x^2+y^2 > 0.15. \end{cases} \tag{64}$$

The interface is a circle $x^2 + y^2 = 0.15$, and Ω^- is the domain inside the circle.

TABLE 10
A grid refinement analysis of the new FD method for the example (63)–(64).

N	N_{dof}	$\|E\|_\infty$	Order	$\|E_D^-\|_\infty$	Order	$\|E_D^+\|_\infty$	Order
34	1089	9.0558E-03		7.9476E+00		1.2503E-01	
66	4225	3.2474E-03	1.55	2.6689E+00	1.65	3.8456E-02	1.78
130	16641	5.3415E-04	2.66	4.2949E-01	2.69	1.0447E-02	1.92
258	66049	1.3746E-04	1.98	2.1659E-01	1.00	2.6409E-03	2.01
514	263169	3.3993E-05	2.03	6.4565E-02	1.76	7.2808E-04	1.87
Average			2.05		1.77		1.89

In Table 10, we show grid refinement results. We see similar patterns of our results as before: second order accurate solution and superlinear convergence for the normal derivatives. Compared with the published infinity error of 1.35×10^{-3} with 404101 nodes in [29], the error of 3.3993×10^{-5} with 263169 nodes obtained from our method is much smaller.

Next, we compare our method with the penalized immersed FEM [1] in which

$$\mathbf{A}^-(x,y) = \begin{pmatrix} 1 & 2 \\ 2 & 5 \end{pmatrix}, \quad \mathbf{A}^+ = \beta\mathbf{A}^-, \qquad \Omega = [-1,\ 1]^2, \tag{65}$$

with $\sigma = 0$, and the analytic solution,

$$u(x,y) = \begin{cases} \beta\left(x^2+y^2\right)^{\frac{3}{2}} & \text{if } x^2+y^2 \le r_0^2, \\ \left(x^2+y^2\right)^{\frac{3}{2}} + (\beta-1)r_0^3 & \text{if } x^2+y^2 > r_0^2, \end{cases} \tag{66}$$

where $\beta > 0$ is a constant and $r_0 = \frac{\pi}{6.28}$. Note that in this example, we have homogeneous jump conditions $[u] = 0$ and $[\mathbf{A}u_n] = 0$. The interface is a circle $x^2 + y^2 = r_0^2$ and Ω^- is the domain inside the circle.

Since the matrix $\mathbf{A}$ is not diagonally dominant, we apply the scaling strategy

$$\mathbf{y} = D_\Gamma \mathbf{x}, \quad D_\Gamma = \begin{pmatrix} 1 & 0 \\ 0 & -\frac{1}{\sqrt{5}} \end{pmatrix}, \quad \mathbf{x} = (x, y)^T, \quad \mathbf{y} = (\bar{x}, \bar{y})^T.$$

Then we apply our method to the transformed problem,

$$-\nabla \cdot \left(\bar{\mathbf{A}} \nabla \bar{u}(\mathbf{y})\right) = \bar{f}(\mathbf{y}), \tag{67}$$

where the new coefficient matrix is

$$\bar{\mathbf{A}}^- = \begin{pmatrix} 1 & -\frac{2}{\sqrt{5}} \\ -\frac{2}{\sqrt{5}} & 1 \end{pmatrix}, \quad \bar{\mathbf{A}}^+ = \beta \bar{\mathbf{A}}^-.$$

In Table 11, we show grid refinement results of the FE-FD method using the same parameters as that in [1] with $\beta = 2.0$. As before, we see similar patterns of our results: second order accurate solution in the infinity norm and superlinear convergence for the normal derivatives. For the purpose of compassion, we also list the result from [1] in Table 12 in which the usual L^2 (second order) and H^1 (first order) are listed. We can see that the two methods have comparable L^2 convergences. Our method has the advantages of pointwise second order convergence for the solution, nearly second order convergence for the normal derivatives, and allowing nonhomogenous jumps in the solution and the flux.

TABLE 11

A grid refinement analysis of the new FE-FD method for the example (65)–(66) *for the purpose of comparison with* $\beta = 2.0$.

N	$\|E\|_\infty$	Order	$\|E\|_{L_2}$	Order	$\|E_D^-\|_\infty$	Order	$\|E_D^+\|_\infty$	Order
34	2.0816E-02		4.7613E-03		1.3140E-01		7.3990E-02	
66	4.9832E-03	2.16	1.2003E-03	2.08	4.7211E-02	1.54	2.4120E-02	1.69
130	1.1105E-03	2.21	2.8588E-04	2.12	1.1962E-02	2.03	6.7150E-03	1.89
258	2.7663E-04	2.03	7.7177E-05	1.91	3.2431E-03	1.90	2.4981E-03	1.44
514	6.5240E-05	2.10	1.8898E-05	2.04	7.6701E-04	2.09	5.9257E-04	2.09
Average		2.12		2.04		1.89		1.78

TABLE 12

A grid refinement analysis of the penalty IFEM for the example (65)–(66) *quoted from* [1] *for the purpose of comparison.*

N	h	$\|E\|_{L_2}$	Order	$\|E\|_{H_1}$	Order
32	1/16	3.859E-03		3.638E-01	
64	1/32	1.009E-03	1.94	1.815E-01	1.00
128	1/64	2.345E-04	2.11	9.196E-02	0.98
256	1/128	5.846E-05	2.00	4.605E-02	1.00
512	1/256	1.459E-05	2.00	2.302E-02	1.00
Average			2.01		1.00

Example 5.5. In this example, we try to mimic the effect of anisotropy on an ideal flow past obstacles or porous media by solving the anisotropic elliptic interface problem with a flow boundary condition. The domain is taken as a square $[-2,\ 2]^2$.

On the left-side boundary $x = -2$, we have a Poiseuille flow profile, $u = u_0(4 - y^2)$—often $u_0 = 1$—and on the right boundary $x = 2$, we have the free flow boundary condition $\frac{\partial u}{\partial n} = 0$. On the bottom and the top boundary, we use a nonslip boundary condition, $u = 0$. The contour plot of the solution is the streamlines of the flow which we do not know. There are no sources in the domain and thus $f = 0$, $w = 0$, and $[\mathbf{A}\nabla u \cdot \mathbf{n}] = v = 0$.

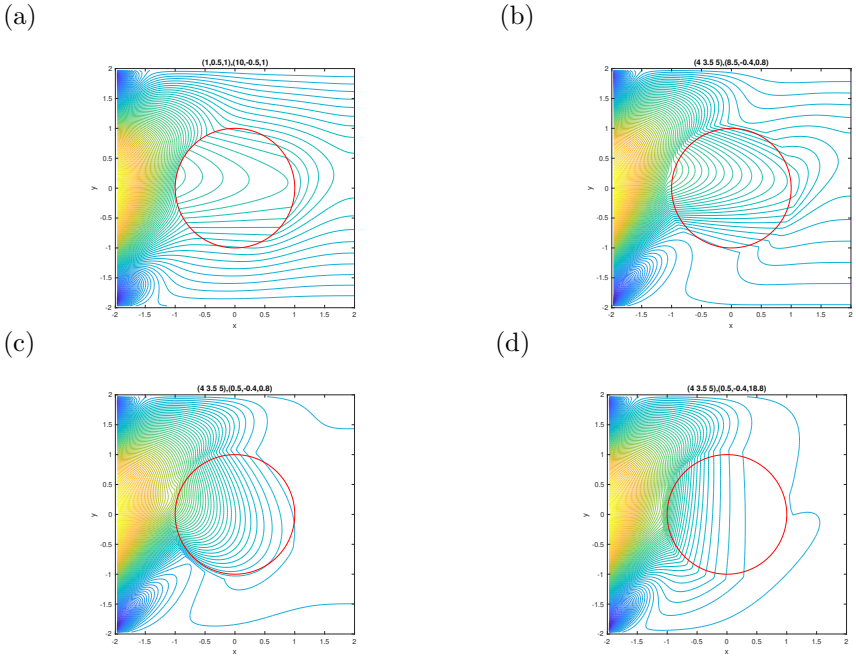

FIG. 4. *Contour plot of a Poiseuille flow through anisotropic materials. The anisotropic matrices are given as* $\mathbf{A}^{\pm} = (a_{11}^{+}, a_{12}^{+}, a_{22}^{+}), (a_{11}^{-}, a_{12}^{-}, a_{22}^{-})$. (a) $(1, 0.5, 1)$, $(10, -0.5, 1)$; (b) $(4, 3.5, 5)$, $(8.5, -0.4, 0.8)$; (c) $(4, 3.5, 5)$, $(0.5, -0.4, 0.8)$; (d) $(4, 3.5, 5)$, $(0.5, -0.4, 18.8)$.

In Figure 4, we show the streamlines (contour plot) of the computed solution u with different anisotropic matrix $\mathbf{A}^{\pm}$ with a unit circle interface. We choose the anisotropic matrix $\mathbf{A}^{+}$ so that the flow has a favorite northeast direction even though the entry velocity profile is in the x- (east) direction. Inside the circular interface, we can choose the anisotropic matrix $\mathbf{A}^{-}$ to obtain the designed flow pattern we wish to see from the plots. In Figure 4(a), A_{11}^{-} is significantly larger than A_{22}^{-}, indicating large variations in the y-direction and the flow changes from northwest to nearly east direction. In Figure 4(b), we adjust the coefficients so that the flow gets more saturated inside the particle while slightly towards southeast direction. In Figure 4(c), the flow becomes nearly circular. In Figure 4(d), A_{22}^{-} is significantly larger than A_{11}^{-} indicating large variations in the x-direction, and the flow changes from northwest to south direction.

In Figure 5, we show simulations results with the same input flow profile and boundary conditions but with a more complicated interface that is given by

$$r(\theta) = 0.75 + 0.2\sin(5\theta), \qquad 0 \le \theta < 2\pi,$$

in polar coordinates. The interface is both convex and concave at different parts of

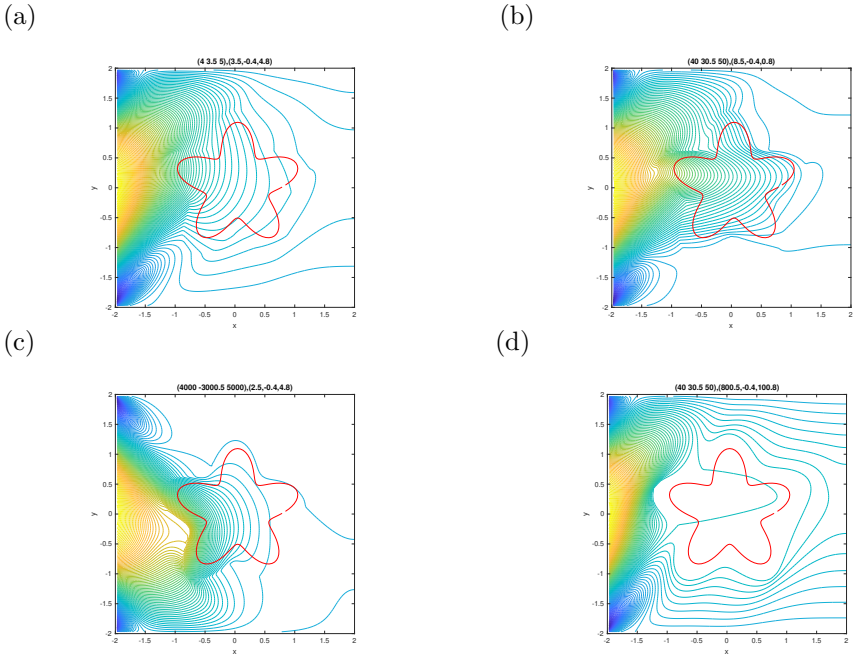

FIG. 5. *Contour plot of a Poiseuille Flow through anisotropic materials. The anisotropic matrices are given as* $\mathbf{A}^{\pm} = (a_{11}^{+}, a_{12}^{+}, a_{22}^{+}), (a_{11}^{-}, a_{12}^{-}, a_{22}^{-})$. (a) $(4, 3.5, 5)$, $(3.5, -0.4, 4.8)$; (b) $(40, 30.5, 50)$, $(8.5, -0.4, 0.8)$; (c) $(4000, 3000.5, 5000)$, $(2.5, -0.4, 4.8)$; (d) $(40, 30.5, 50)$, $(800.5, -0.4, 100.8)$.

the interface with varying curvature. Not only can we control the flow pattern both inside and outside using different anisotropic matrix $\mathbf{A}^{\pm}$, we can also see how the curvature affects the flow. In Figure 5(b), the flow inside changes the directions and gets saturated. In Figure 5(c), we alter the flow direction from east at the entrance to southeast in contrast to Figure 5(b). In Figure 5(d), we show a big jump in the magnitude of the anisotropic matrix $\mathbf{A}$; the start-particle almost becomes an obstacle.

6. Conclusions. In this paper, a new finite difference method has been developed for anisotropic elliptic interface problems based on Cartesian meshes. At regular grid points, the finite difference equations are derived from the standard finite element (P1) discretization, while at irregular grid points the finite difference equations are derived from the maximum preserving IIM. The linear system of equations is typically block tridiagonal with seven nonzeros for regular grid points, while nine for irregular ones. Error analysis using finite element (P1) and finite difference theories shows that the method is second order accurate except for a factor of $|\log h|$. Numerical results show that not only is the computed solution second order globally, but also its normal derivative at the interface from two sides of the interface. We believe that our method can be expanded to random interface problems; see, for example, [3, 12, 13, 14].

REFERENCES

[1] N. AN AND H. CHEN, *A partially penalty immersed interface finite element method for anisotropic elliptic interface problems*, Numer. Methods Partial Differential Equations, 30 (2014), pp. 1984–2028.

[2] I. BABUŠKA, *The finite element method for elliptic equations with discontinuous coefficients*, Computing, 5 (1970), pp. 207–213.

[3] G. Bao, Y. Cao, Y. Hao, and K. Zhang, *First order second moment analysis for the stochastic interface grating problem*, J. Sci. Comput., 77 (2018), pp. 419–442.
[4] S. Bergmann, K. Albe, E. Flegel, D. A. Barragan-Yani, and B. Wagner, *Anisotropic solid-liquid interface kinetics in silicon: An atomistically informed phase-field model*, Modelling Simul. Mater. Sci. Eng., 25 (2017), 065015.
[5] D. Braess, *Finite Elements: Theory, Fast Solvers, and Applications in Solid Mechanics*, 3rd ed., Cambridge University Press, Cambridge, UK, 2007.
[6] J. H. Bramble and V. Thomée, *Interior maximum norm estimates for some simple finite element methods*, ESAIM Math. Model. Numer. Anal., 8 (1974), pp. 5–18.
[7] S. Brenner and L. Scott, *The Mathematical Theory of Finite Element Methods*, Springer, New York, 2002.
[8] D. De Zeeuw, *Matrix-dependent prolongations and restrictions in a blackbox multigrid solver*, J. Comput. Appl. Math., 33 (1990), pp. 1–27.
[9] M. A. Dumett and J. P. Keener, *An immersed interface method for solving anisotropic elliptic boundary value problems in three dimensions*, SIAM J. Sci. Comput., 25 (2003), pp. 348–367, https://doi.org/10.1137/S106482750240697X.
[10] M. Dumett and J. Keener, *An immersed interface method for anisotropic elliptic problems on irregular domains in* $2D$, Numer. Methods Partial Differential Equations, 21 (2005), pp. 397–420.
[11] L. C. Evans, *Partial Differential Equations*, 2nd ed., Grad Stud. in Math. 19, AMS, Providence, RI, 1998.
[12] Y. L. Hao, F. D. Kang, J. Z. Li, and K. Zhang, *A numerical method for Maxwell's equations with random interfaces via shape calculus and pivoted low-rank approximation*, J. Comput. Phys., 371 (2018), pp. 1–18.
[13] H. Harbrecht and J. Li, *First order second moment analysis for stochastic interface problems based on low-rank approximation*, ESAIM Math. Model. Numer. Anal., 47 (2013), pp. 1533–1552.
[14] H. Harbrecht, R. Schneider, and C. Schwab, *Sparse second moment analysis for elliptic problems in stochastic domains*, Numer. Math., 109 (2008), pp. 385–414.
[15] S. Hou, P. Song, L. Wang, and H. K. Zhao, *A weak formulation for solving elliptic interface problems without body fitted grid*, J. Comput. Phys., 249 (2013), pp. 80–95.
[16] S. Hou, W. Wang, and L. Wang, *Numerical method for solving matrix coefficient elliptic equation with sharp-edged interfaces*, J. Comput. Phys., 229 (2010), pp. 7162–7179.
[17] T. Hou, X. Wu, and Y. Zhang, *Removing the cell resonance error in the multiscale finite element method via a Petrov-Galerkin formulation*, Commun. Math. Sci., 2 (2004), pp. 185–205.
[18] W. Huang and S. I. Rokhlin, *Interface waves along an anisotropic imperfect interface between anisotropic solids*, J. Nondestructive Evaluation, 11 (1992), pp. 185–198.
[19] H. Ji, Q. Zhang, and B. Zhang, *Inf-sup stability of Petrov-Galerkin immersed finite element methods for one-dimensional elliptic interface problems*, Numer. Methods Partial Differential Equations, 34 (2018), pp. 1917–1932.
[20] V. I. Levitas and J. A. Warren, *Phase field approach with anisotropic interface energy and interface stresses: Large strain formulation*, J. Mech. Phys. Solids, 91 (2016), pp. 94–125.
[21] Z. Li and K. Ito, *Maximum principle preserving schemes for interface problems with discontinuous coefficients*, SIAM J. Sci. Comput., 23 (2001), pp. 1225–1242, https://doi.org/10.1137/S1064827500370160.
[22] G. B. McFadden, A. A. Wheeler, R. J. Braun, S. R. Coriell, and R. F. Sekerka, *Phase-field models for anisotropic interfaces*, Phys. Rev. E, 48 (1993), pp. 2016–2024.
[23] K. W. Morton and D. F. Mayers, *Numerical Solution of Partial Differential Equations*, Cambridge University Press, Cambridge, UK, 1995.
[24] K. Schittkowski, *QL-quadratic Programming, version* 1.5, 1991, https://www.uni-bayreuth.de/departments/math/~kschittkowski/ql.htm.
[25] R. Scott, *Optimal* L^∞ *estimates for the finite element method on irregular meshes*, Math. Comp., 30 (1976), pp. 681–697.
[26] Z. Suo, *Singularities, interfaces and cracks in dissimilar anisotropic media*, Proc. Roy. Soc. Edinburgh Sect. A, 427 (1990), pp. 331–358.
[27] F. Tong, W. Wang, J. Zhao, X. Feng, and Z. Li, *How to obtain an accurate gradient for interface problems?*, J. Comput. Phys., 405 (2020), 109070.
[28] N. G. Tuncel and A. H. Serbest, *Reflection and refraction by an anisotropic metamaterial slab with diagonal anisotropy*, in Proceedings of the IEEE International Conference on Microwaves, Communications, Antennas and Electronic Systems (COMCAS), IEEE, 2015, pp. 1–4.

[29] L. Wang, S. Hou, and L. Shi, *A numerical method for solving elliptic interface problems using Petrov-Galerkin formulation with adaptive refinement*, Math. Probl. Eng., 2018 (2018), 3721258.
[30] R. E. White, *An Introduction to the FE Method with Applications to Non-linear Problems*, John Wiley & Sons, Chichester, UK, 1985.
[31] H. Wu, *L^∞-error Estimate for Immersed Finite Element Methods*, private communication, 2015.
[32] W.-J. Ying and C. S. Henriquez, *A kernel-free boundary integral method for elliptic boundary value problems*, J. Comput. Phys., 227 (2007), pp. 1046–1074.